Multifunctional Applications of a Novel Ru-Metal Mixed PVAL Flexible Composite for Limiting Absorption and Varistor: Synthesis, Optical, and Electrical Characterization

H. Elhosiny Ali[1,2,3] · M. M. Abdel-Aziz[1,4] · H. Algarni[1] · I. S. Yahia[1,3,5] · Yasmin Khairy[2]

Abstract

Composite films with vital multifunctional properties for optoelectronic and varistor applications were prepared via casting procedures. Herein, the present novel composites are based on semi-crystalline polyvinyl alcohol, PVAL, mixed with different contents of Ruthenium-metal. The structure of the films has been fully identified through Fourier Transform (FT-IR), diffraction analysis of X-ray (XRD), and microscopy of scanning electron (SEM). They confirm significant interactions between Ru-metal and PVAL, which leads to a decrease in polymer crystallinity. Ru-metal's impact on the optical performance has been studied using spectroscopy of UV–Vis–NIR, whereas the applicability of these films for varistor devices was investigated by measuring the electrical conductivity and I–V curves. The crystallite length (D), the spacing of interplanar (d), dislocation density (δ), internal strain (ε), and separation of interchain (R) parameters were calculated from the measurement of XRD. The active absorption band in FTIR spectra shows a significant interaction of Ru-metal with the PVAL via OH groups. The cluster of metal on the composite surface increases with the doping concentration, as illustrated via SEM. Optical bandgaps (E_{gi} & E_{gd}) are estimated from Tauc and absorption fitting (ASF) are nearly equal and reduced with ruthenium addition. Limiting optical absorption (LOA) performance tested using two laser sources showing the reduction of optical transmission via high doping concentration films. With rising Ru-metal content and frequency, the dielectric and AC conductivity tends to be enhanced. Also, the I-V characteristic was improved, and the conductivity follows the fitting of Jonscher. The collected result reflects the consideration of flexible Ru/PVAL as a promising polymeric film in varistor, micro-optics, optical fibers, and CUT-OFF laser applications.

Keywords Ru-metal doped PVAL film · XRD analysis · Gaussian fitting · FT-IR spectroscopy · SEM · EDX · Limiting optical absorption · Electrical performance

✉ Yasmin Khairy
yasminphysics@gmail.com; yasmin_ph@zu.edu.eg

1   Advanced Functional Materials & Optoelectronic Laboratory (AFMOL), Department of Physics, Faculty of Science, King Khalid University, P.O. Box 9004, Abha, Saudi Arabia

2   Physics Department, Faculty of Science, Zagazig University, Zagazig 44519, Egypt

3   Research Center for Advanced Materials Science (RCAMS), King Khalid University, P.O. Box 9004, Abha, Saudi Arabia

4   Department of Physics, Faculty of Science, Al-Azhar University, Nasr City, Cairo, Egypt

5   Nanoscience Laboratory for Environmental and Biomedical Applications (NLEBA), Semiconductor Lab., Physics Department, Faculty of Education, Ain Shams University, Roxy, Cairo, Egypt

1 Introduction

Polymers doped with metal particles were used over the recent decades in numerous applications, such as high energy rechargeable batteries, micro-optics, optoelectronics, fuel cells, microelectronic devices, and several other applications [1–3]. The characteristics of polymer-inorganic composites are directly related to the particle concentration, chemistry, size, and dispersion in the polymer matrix [4]. The presence of a few amounts of inorganic particles within the polymeric matrix will enhance the mechanical, thermal, optical, and electrical characteristics of polymer materials allowing new polymer composite materials of high quality [4, 5]. S. Daikh et al. shows an increment in the conductivity of the (HCl–ZnCl$_2$) doped PANI/ZnO film to 0.081 S.cm^{-1} [6]. Ali et al. have reported that the optical bandgap of PVAL was reduced to

4.55 eV by adding 20 wt % of $La(NO_3)_3 6H_2O$ salt [2]. The essential factor of enhancing the polymeric material characteristics is the transition from insulating materials to conducting activity by introducing ionic solid [1].

Moreover, Poly (vinyl alcohol) (PVAL) has been a significant subject of interest in many of the polymers due to their fascinating properties and industrial applications, such as surgical instruments, architecture, electronics, and food packaging [7]. Additionally, PVAL contains a carbon chain as backbone and hydroxyl groups that could be an H-bonding source, allowing polymer composite to be formed. Therefore, PVAL has generally been considered a suitable host material [8, 9]. PVAL is a semi-crystalline polymer. If it is doped with an appropriate dopant, the particles will interact in the amorphous or crystalline part of the polymer. The structural, electrical, and optical characteristics of the PVAL will change in both cases [10]. The semi-crystalline polymer contains tiny free volume holes that have been generated inside the polymer matrix in chain-folds due to the irregular packing of molecules in the amorphous phase. Such free-volume holes significantly affect the polymer's structural, electrical, and optical characteristics [10]. It was found that after the addition of Na_2Co_3, the H-bonding interaction among PVAL and CMC (Carboxyl methylcellulose sodium) raised and the crystallinity degree of PVAL reduced [11]. Also, the PVAL with a high concentration of Er^{3+}, Y^{3+}, and La^{3+} increased the interactions and improved the optical, dielectric, and electrical properties of the polymer [12–14].

An improvement of PVAL properties in previous work was explained based on inorganic production (such as Fe^{3+}, Tb^{3+}, $CrCl_3$, and $CuCl_2$) particles embedded in polymers [15–18]. Considerable enhancement in the morphological, optical, and electrical features led to the polymer's use in many appropriate fields. Ruthenium is a rare transition metal that belongs to inorganic compounds and no previous work with polymer was studied. This research aims to improve the structural, optical, and electrical characteristics of the PVAL film by embedding Ru-metal through it as a novel composite material. Moreover, the critical optical parameters were determined. The composite had been performed using the solution casting method, which led to the development of high-quality PVAL/Ru films. Finally, various spectroscopic and microscopic methods such as XRD, FT-IR, SEM, EDAX/EDS, UV–Visible–NIR, ac-electrical conductivity, and dielectric performance were briefly discussed and compared with other published composites.

2 Experimental

2.1 Preparation of PVA/Ru Composite

4 N purity host polymer PVAL has been purchased from Alfa Aeaser, Karsruhe, Germany, as a commercial product.

For doping purposes, flammable solid ruthenium (99.9% purity) has come from the Aldrich chemistry company. 45 g of PVAL has been dissolved in one liter of deionized water with continuous stirring at 100 °C till the solution becomes completely homogeneous, and a viscous solution developed. The solution casting technique was used to produce PVAL: Ru composite with concentrations 0, 0.001, 0.005, 0.01, 0.1, and 0.5 g on 60 ml of PVAL. The mixtures have been agitated in ultrasonic for 2 min. Homogeneous composite solutions have been poured into Petri-glass plates. The oven was set at a temperature of 35 °C for 96 h. The as-prepared samples have been peeled off after evaporation. Homogenous and dark color films were collected with an average thickness of 0.1 mm. The samples will be named as follows: PVAL:0 wt.% Ru (RPVA-0), PVAL:0.037 wt.% Ru (RPVA-1), PVAL:0.1845 wt.% Ru (RPVA-2), PVAL:0.369 wt.% Ru (RPVA-3), PVAL:1.818 wt.% Ru (RPVA-4), PVAL:3.57 wt.% Ru (RPVA-5), and PVAL:15.63 wt.% Ru (RPVA-6). The weight (wt.%) of Ru metal in the PVAL matrix have been calculated using the following formula:

$$w_{Ru}(\%) = \frac{w_{Ru} \times 100}{w_{Ru} + w_{PVAL}} \tag{1}$$

where w_{Ru} and w_{PVAL} are representing the weights of ruthenium and PVAL, respectively.

2.2 Experimental Setup

The Fourier transformation infrared (FTIR) transmission spectrum for pristine PVAL and PVAL/Ru composite was accomplished by a Thermo Nicolet 67,600 FTIR spectrometer wavenumber range 4000–500 cm^{-1}. Shimadzu XRD-6000 diffractometer CuK_α with wavelength $\lambda = 1.5418$ Å, was used for measuring the X-ray spectra of the as-prepared samples, in the diffraction range $10° \leq 2\theta \leq 60°$.

The as-prepared film surface morphology properties have been examined using a scanning electron (SEM) microscope (JSM-6360). Moreover, the SEM survey of energy-dispersive X-ray analysis (SEM-EDAX) and mapping analysis of SEM-energy dispersive spectroscopy (SEM–EDS) can be used to analyze the composition and distribution of Ru in the PVAL network.

Spectrum transmission and absorption measurements have been studied at room temperature in the range 200–2500 nm with the help of the UV–Visible–NIR JASCO V-570 spectrometer.

The limiting absorption properties in the Vis region for Ru: PVAL films were measured via two kinds of lasers, (I) He–Ne laser with $\lambda = 632.8$ nm and power of 0.5 mW, as well as (II) green laser (Baran laser company) of $\lambda = 533$ nm and medium power 15.396 mW. Each tested film was fixed at 0.1 m (the focal length of the lens) during the measurement.

Both the lens and the sample were fixed in the front of the entering and the output beams. For detecting the power of the output, a power meter with digital sensitivity was used.

AC-conductivity and dielectric were analyzed using a semiconductor KEITHLEY 4200-SCS at room temperature and frequency oscillating between 30 kHz and 10 MHz.

3 Results and Discussion

3.1 Fourier Transform Infrared (FTIR) Analysis

Infrared spectroscopy can recognize how polymer chains interact with filler material. Figure 1 displays the transmission spectra of pristine and Ru doped PVAL with multiple concentrations 0.037, 0.185, 0.37, 1.85, 3.7, and 18.5 wt.% of Ru, which was evaluated in the range 4000–500 cm^{-1}. For pristine PVAL, a reliable transmission band centered at a wavenumber of 3328 cm^{-1} is probably due to the OH group's stretching vibrations. CH stretching symmetric vibration is attributed to the band placed at 2882 cm^{-1} within the PVAL [19]. Furthermore, the doping concentration-dependent location and intensity of such IR transmission peaks show the structural modification in the PVAL polymer backbone [20]. The intensity of the transmitted peaks is drastically decreased for more Ru-metal levels associated with the change in molecular arrangement via hydroxyl bonds. Such a concept proves the presence of a disordered formation inside the PVAL structure [21]. The transmission peak evaluated at 2179 cm^{-1} has been recognized in all the FTIR spectra of the as-prepared films related to the -CH$_2$ stretching mode of symmetric vibration. The band at 1722 cm^{-1} is generally ascribed to the stretching vibration of the carbonyl C = O
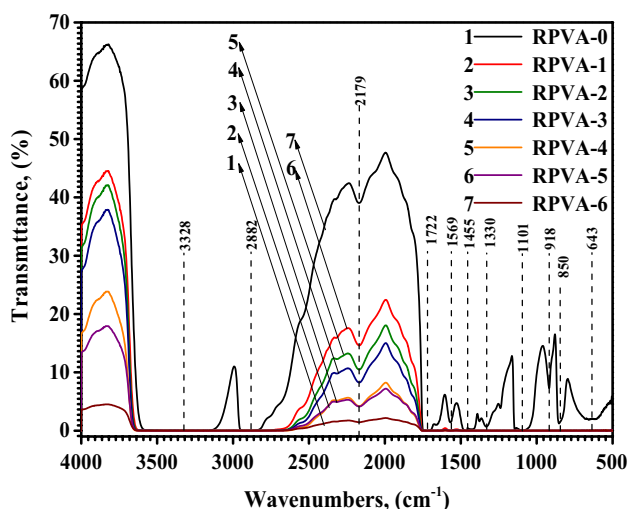
[22]. Furthermore, the transmittance band at 1569 cm^{-1} has been related to OH or CH bending's existence of vibrations. The bands at 1455 and 1330 cm^{-1} were associated with the bending and wagging of CH$_2$ vibrations. Nevertheless, the observed band centered at 1101 cm^{-1} is commonly taken as a measuring technique for investigating PVAL's crystalline structure and accompanying with acetyl groups C–O stretching. Many previous research types show that the 1101 cm^{-1} narrowing band significantly affects crystallization improvement in the PVAL matrix. The rise in peak strength at this band had been suggested as considerable evidence of the polymer's crystallization degree [23]. On the other hand, as the filler concentration of Ru increases, the bandwidth centered at 1101 cm^{-1} increases, while its intensity decreases and disappears completely. The doping of Ru to PVAL structure causes a cross-linking interaction and raises the amorphous ratio [24]. Other vibrational bands at 918, 850, and 643 cm^{-1} have been associated with C–C stretching, -CH out of plane vibration, and C-H stretching, respectively [16]. A similar influence was observed by doping PVAL with CdS nanoparticles [25].

3.2 X-Ray Diffraction and Structural Variables

The X-ray investigation has checked the structure of pristine and Ru doped PVAL films. The films' patterns with different concentrations (0.037, 0.1845, 0.369, 1.818, 3.57, and 15.63 wt% Ru) are illustrated in the diffraction angle range $10° \leq 2\theta \leq 60°$ (Fig. 2). A broad diffraction peak at 20.030° refers to (101) reflection of monoclinic crystal with d spacing 4.430 Å. This plane ascribed to the intermediate nature between the amorphous and the crystalline phases of the pristine film [15]. A further broad and low-intensity peak at 40.50° was observed, referring to non-crystalline regions in a polymer network [26]. The crystalline peak of PVAL diffraction was possibly reduced drastically and shifted slightly to higher angles with the gradual addition of Ru-metal. However, the peak of non-crystalline PVAL regions disappeared due to Ru-ion's interstitial sites within the PVAL network connected with the hydrogen bond via the charge transportation. It is understood that PVAL's crystalline structure derives mainly from the tight intermolecular communication among chains across the molecular bonding of H [27]. No other or high-pitched peaks were observed in the XRD of PVAL–Ru that suggest a close contact, in the polymer PVAL environment, between the chains and Ru-ions except the film containing high concentrations (15.63 wt%). For PVAL:18.5 wt% Ru film, the Bragg peak for fcc type of Ru equivalent to (111) plane was observed at ~ 31.975° [28].

The crystallite size (D), and the interplanar spacing (d) were calculated using Scherer's equation $D = (k\lambda/\beta cos\theta)$ and Bragg's law $d = (n\lambda/2sin\theta)$, respectively [29], whereas the strain (ε) can be calculated from the relation

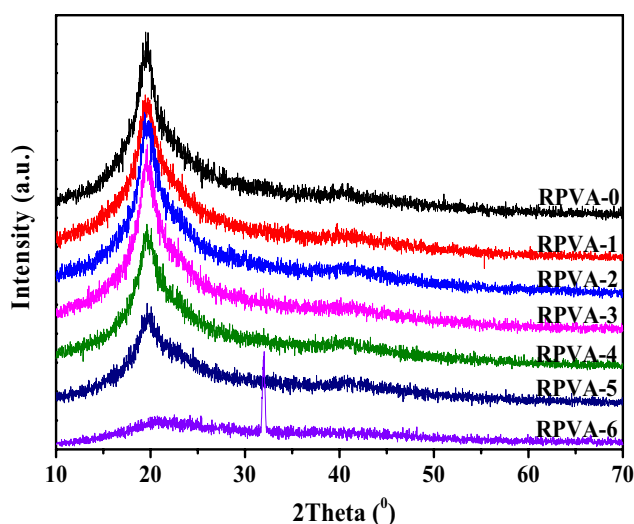**Fig. 1** FTIR transmittance spectra of unmixed PVAL and Ru mixed PVAL polymer films

Fig. 2 XRD patterns of unmixed PVAL and Ru mixed PVAL polymer films

$\varepsilon = (\beta / 4 tan\theta)$ [10]. The average separation of the interchain in the amorphous zone has been calculated using the equation $R = (5\lambda / 8 sin\theta)$ [30] and the dislocation density via the relation $\delta = (1/D^2)$ [29]. k is a constant = 0.9, λ is the incident X-ray beam's wavelength, θ is the angle between the incident ray and the scattering plane. β is the full width at half maximum (FWHM) for the absolute peak of pristine and Ru doped films that were assessed from the Gaussian fitting of the prominent PVAL peak, as shown in Fig. 3a–d. The calculated structural parameters are summarized in Table 1. With an increment of the Ru dopant concentration, the FWHM values increased, which attributes to the reduction in the crystallite size of composites compared to the pristine PVAL. The induced strain increased with filler concentration in the polymer. This indicates the distortions and imperfections in PVAL polymer films for more wt% of Ru-metal. Besides, it has been shown that the average inter-chain separation suggests the weak intermolecular hydrogen bonding that allows the molecular movements to disappear, which produces a drop in crystallinity [31]. However, the density of the dislocation improves with rising concentrations of filler. Such results indicate that the composite PVAL-Ru development towards irregularity of chains is probably attributed to the Ru-ions that generate additional bonds within the amorphous region between the neighboring chains. Z. A. Alrowaili et al. found that as the ratio of carmine dye increases in the PVAL, the amorphous peak increases, and the crystal structures changed [32].

3.3 SEM, EDS, and EDX Examination

SEM (scanning electron microscope) technique has been used to examine the surface morphology of pristine and

Ru-doped PVAL polymers films (see Fig. 4a–f) with varying concentrations of Ru-filled PVAL films. PVAL network is detected as a gray region, whereas bright semi-spherical aggregates contribute to Ru particles in the composite surfaces, as seen in the SEM pictures. In the as-prepared composite of low-level Ru, the nucleating operator promotes the polymer's structural organization that always creates smaller crystals. Moreover, crystals with larger sizes were produced, and the surface microstructure of the as-prepared polymer PVAL: Ru samples were irregular by introducing Ru in higher content to the PVAL matrix. Consequently, because of the full surface area with a larger cluster size, the transmission could be further avoided, which often contributes to improved light absorption. This result can be comparable with that observed by doping PVAL with Mn_2O_3 nanoparticles [26]. The nanoparticles agglomerated with increasing the doping ratio in PVAL.

The as-prepared composite's chemical composition has been distinguished by using energy dispersive X-rays analysis (EDX). Figure 5 and its inset illustrate the distribution of the elements (EDS mapping) and the composition peaks of C, O, and Ru elements (EDX) of the as-prepared RPVA-1 sample. It shows that only Ru, C, and O elements were observed in the PVAL matrix without further impurities. The weight percentage was 36.90, 33.78, and 29.32 for the carbon, oxygen, and ruthenium in the as-prepared film. The number of atoms of the specified element to the total number of atoms was 56.13, 38.5 7, and 4.30 for the same atoms.

3.4 Optical Study in the UV to IR Range

Analysis of optical parameters from UV to IR plays a crucial role in detecting and describing changes in internal band structure by observing electronic transitions within the polymeric PVAL material.

3.4.1 Optical Transmission (*T*) and Absorption (*A*)

The measurement optical *T* and *A* for unmixed and mixed PVAL with a weight vary from 0.037 to 18.5 wt% of *Ru*-metal, in the spectral range 200—2500 nm, are shown in Fig. 6a, b. It is shown that PVAL film has a maximum transmission of approximately 95% and drops dramatically to zero with a rise in Ru-dopant concentration up to 18.5 wt.%. This consequence was explained in numerous papers for example a certain Mn_2O_3 or CeO particles percentages significantly reduces the transmission of light for PVAL [26, 33]. For all present polymeric samples in the UV area, there is a slight shoulder peak at ~288.74 nm, which is based on the presence, via the host polymer network, of an electronic transition from n to π^* linked to a carbonyl bond (C = C) [16]. Also, a tiny absorbing band with a peak of approximately 325 nm was observed, assigned to the electronic
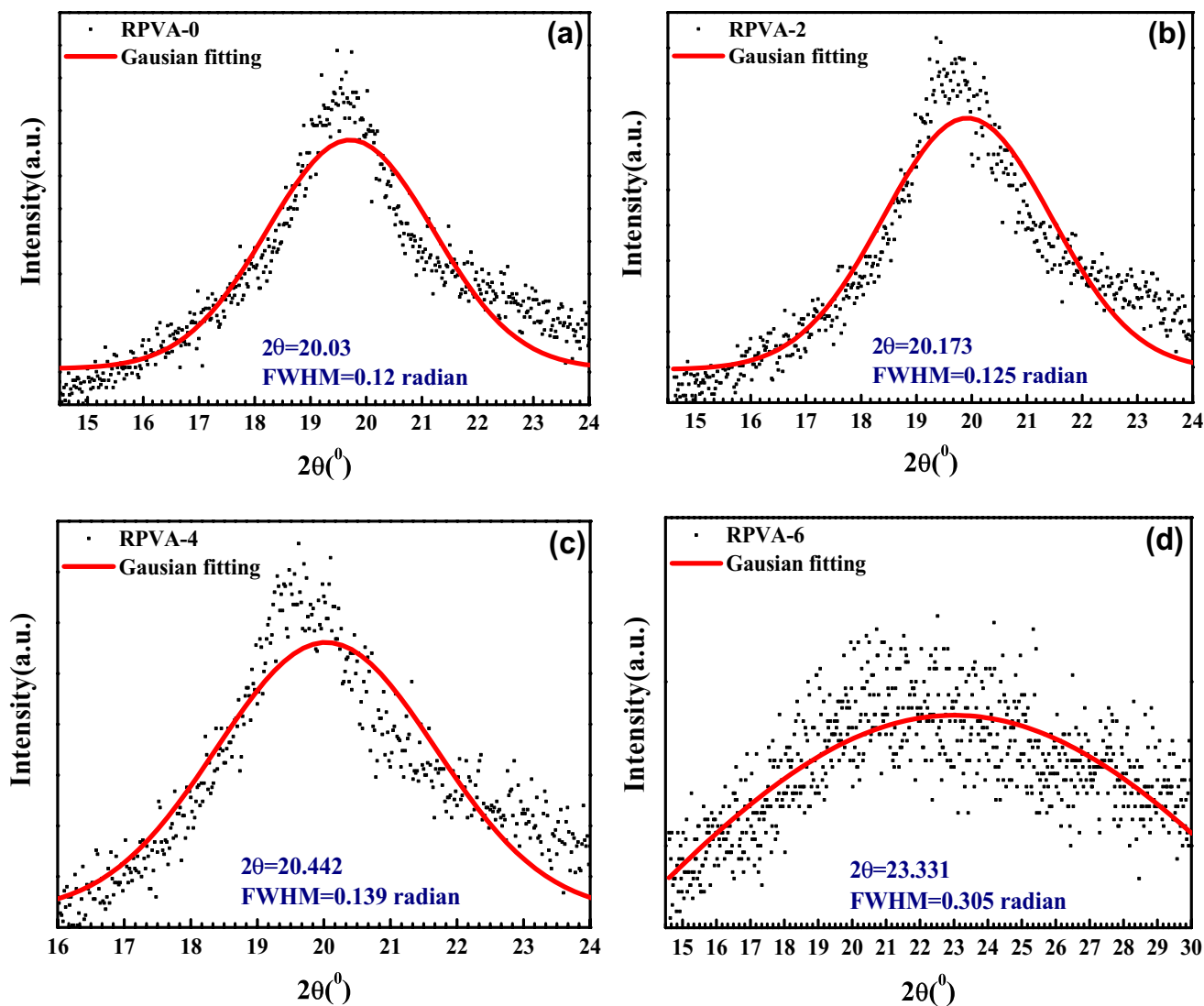
Fig. 3 Gaussian fitting of the main XRD peaks of unmixed and Ru mixed PVAL films

Table 1 The determined structural parameters of pristine and Ru doped PVAL polymer films

Films	Peak (101)						
	$2\theta^o$	β (rad)	D (nm)	d (Å)	ε	R (Å)	$\delta \times 10^{17}$ (lines/m^2)
RPVA-0	20.030	0.120	1.174	4.430	0.170	5.541	7.255
RPVA-1	20.169	0.124	1.137	4.400	0.174	5.503	7.859
RPVA-2	20.173	0.125	1.128	4.399	0.176	5.502	7.735
RPVA-3	20.233	0.129	1.093	4.386	0.181	5.486	8.371
RPVA-4	20.442	0.139	1.014	4.342	0.193	5.431	9.726
RPVA-5	20.970	0.145	0.973	4.233	0.196	5.295	10.563
RPVA-6	23.331	0.305	0.465	3.810	0.369	4.766	46.248

transition π-π* of the unsaturated carbonyl bond (C=O) [34]. There are no absorption peaks in the visible wavelength, suggesting that PVAL doped films have high pureness of optical efficiency [35]. An increase in the absorption rate measured throughout the entire spectrum was observed for films doped with Ru-metal, as this progress increases with the concentration of dopants. The absorption activity's increase can be taken as proof of the typical interaction

Fig. 4 SEM pictures of the as-prepared PVAL films doped with **a** 0.037, **b** 0.185, **c** 0.37, **d** 1.85, **e** 3.7, and **f** 18.5 wt% Ru-metal
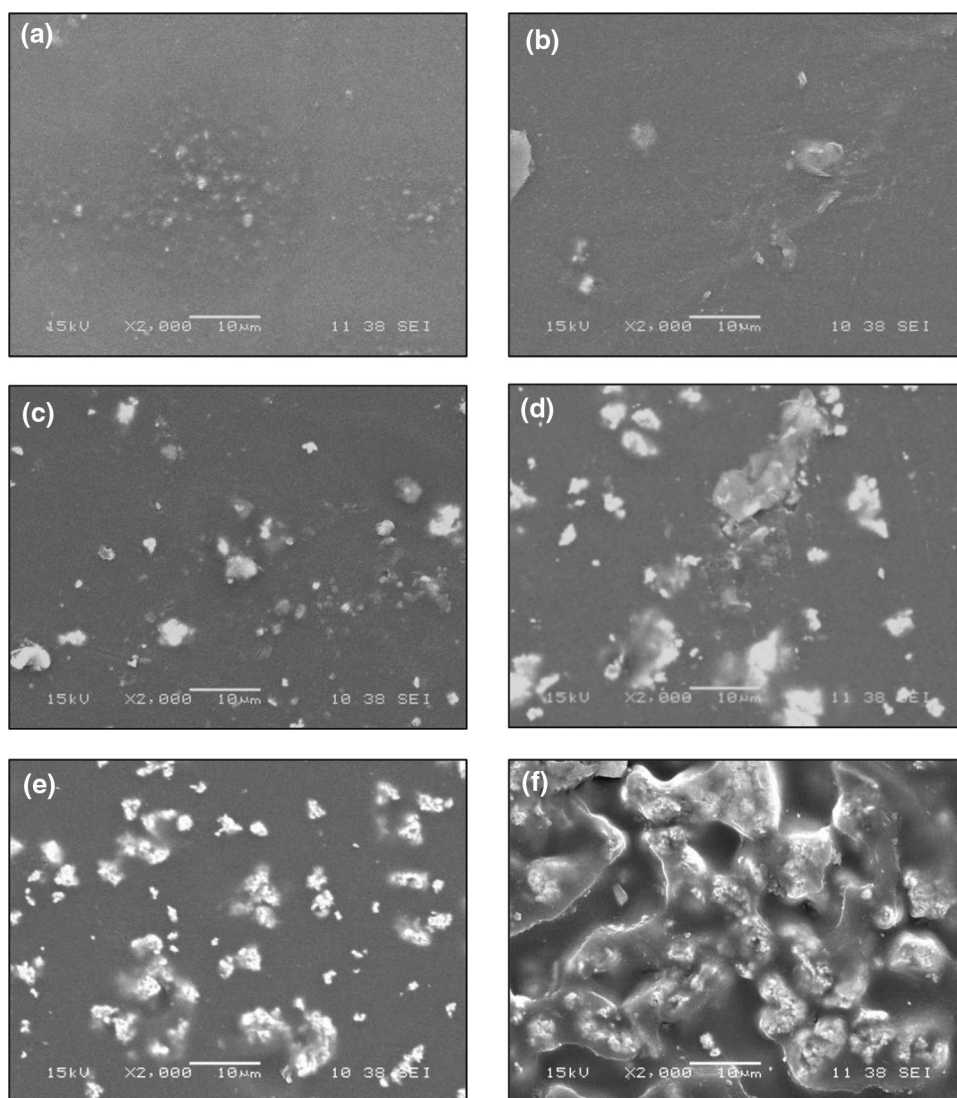
of the Ru-particles with the polymer network. It can be described as the premise of creating new intermolecular bonds via OH⁻ anions across the entire polymer backbone network. This results in a modification due to new defects that result in the formation of new bandgap levels by augmentation of the Ru-dopant concentration. The improvement in the absorption values for polymer films with increased Ru concentrations from 0.037 wt% to 18.5 wt% correlates to a reduction in the transmittance values, as plotted in Fig. 6a. A plausible explanation for this attitude is that the internal structure's modification mechanism enhances the number of disorders and defects. This increases the possibility of light scattering and reducing transmission [36–38]. The maximum value of optical absorption for PVAL mixed with 18.5 wt% Ru. It is possible to grant a strong electronegativity of Ru, which was doped in the polymer network. The increase in electronegativity increases the absorption and reduces our sample transmission [39, 40].

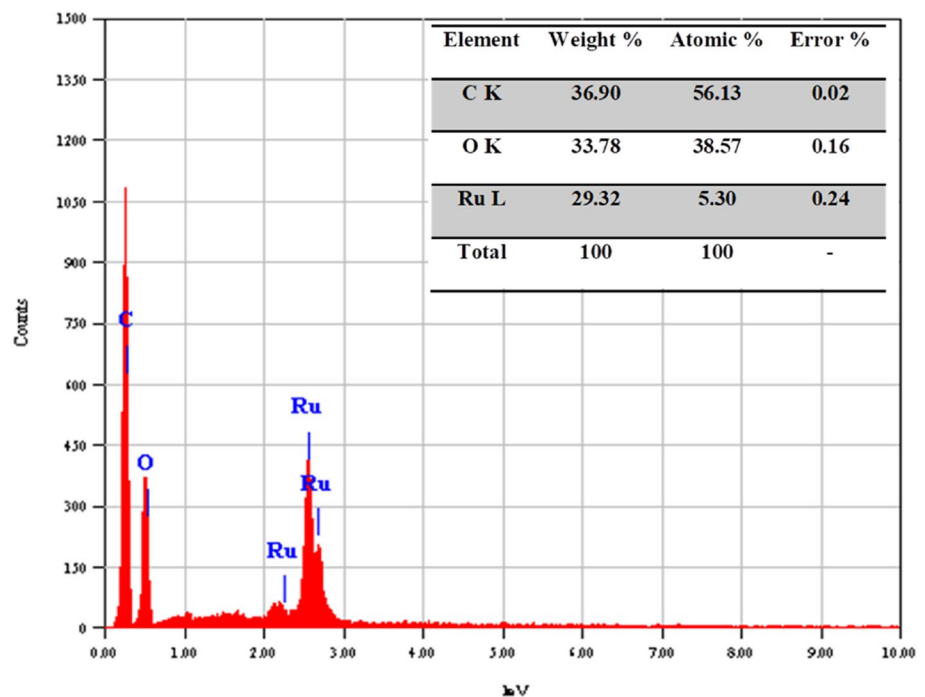### 3.4.2 The Optical Absorption Coefficient and Localized State Width

The optical absorption coefficient (α) enables a clarification concerning the solid material's electronic band structure. It is one of the fundamental parameters depending on the incident wavelength. The coefficient of absorption was determined from the spectra of the following formula [41–43]:

$$\alpha = \frac{Abs.}{t} \times 2.303 \tag{2}$$

where t is the film's thickness. The α value near the absorption edge is exponentially dependent on the energy of the photon $h\nu$ incident and is based on Urbach's relation [44]:

$$ln\alpha = ln\alpha_o + \frac{h\nu}{E_u} \tag{3}$$

Fig. 5 The energy dispersive X-ray analysis (EDX) for RPVA-1 film

Element	Weight %	Atomic %	Error %
C K	36.90	56.13	0.02
O K	33.78	38.57	0.16
Ru L	29.32	5.30	0.24
Total	100	100	-

where α_o is constant, and E_u is the Urbach energy or the optical activation energy. The practical study of the absorption edge supplies precious knowledge about the gap in the optical band. As an electron is excited from the lower to the higher energy levels, the edge of absorption is measured in the process of absorption [45]. Figure 7 represents the variation of α with the photon energy ($h\nu$) before and after mixing with Ru-metal. The α values increase with the Ru ratio due to increased interaction between the OH groups in the PVAL network and dopant-ions. The presence of Ru-ions inside the PVAL polymeric material decreases the OH group density. The location of the edge of the absorption E_e has been calculated by linear extrapolation to zero absorption coefficient ($\alpha = 0$), as plotted in Fig. 7. The absorption edge moves to lower values from 5.347 eV for unmixed PVAL to 4.675 eV for RPVA-6, as recorded in Table 2. This decrease is due to the formation of localized states in the prohibited gap associated with the increase of Ru [39]. The minor changes of the absorption edge are due to the complexity of Ru-ions in the PVAL network. The E_e result in this issue is consistent with that obtained for PVAL: La^{3+} polymer by Ali et al., where the absorption edge changes from 5.12 to 4.59 eV by adding 20 wt% of $La(NO_3)_3 6H_2O$ salt [2].

In disordered materials, the Urbach tail should have been identified. It is useful to recognize the characteristics of electronic transportation. The size of the Urbach tail is a representation of the degree of defects in the prohibited gap or the space separating the valence and the conduction bands [46, 47]. Figure 8 displays plots of $ln\alpha$ vs. the energy $h\nu$. The interpolate shows variation in Urbach energy, E_u, depending on the doping Ru concentration in the PVAL. Table 2 lists the values of E_u for each examined polymer film obtained from the slope for the fitted curves' linear area. Their values are compatible with some other materials recorded earlier [48, 49] which prove further defects in the composite films. The Urbach energy increased for composite with increasing the Ru-particles in PVAL. This result suggests the development of localized states within the prohibited bandgap.

3.4.3 Determination of Optical Bandgap via Different Methods

Polymeric materials of low bandgap have attracted significant scientific and technical attention for designing and manufacturing of beneficial photovoltaic instruments due to the high similarity between the absorption spectrum of the low bandgap polymers and the solar spectrum [50]. The absorption phenomenon depends on the photon with a sufficient amount of energy to allow electrons to transfer from low-energy of valence bands to high-energy of conduction bands. In a similar k-space, electron excitement leads to the direct transition from the valence into the crystalline materials' conduction bands. Also, the electron hopping in the conduction band in various *k*-spaces produces indirect transitions. The Davis-Mott models presume that the wave function is localized, and the probability of transition depends upon overlapped wave functions. A localized state spreads into the band gap from the conduction band and the valence band for polymer-based materials. This localized state can, therefore, influence the electron transition [51].
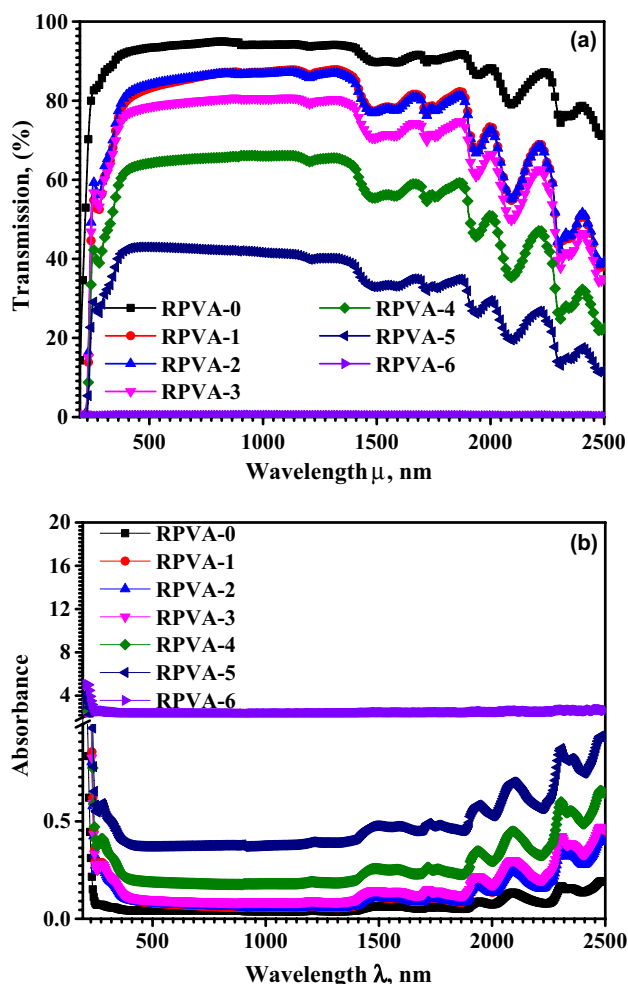
Fig. 6 The UV–Visible–IR spectra of pristine PVAL and Ru doped PVAL films, **a** transmittance and **b** absorbance
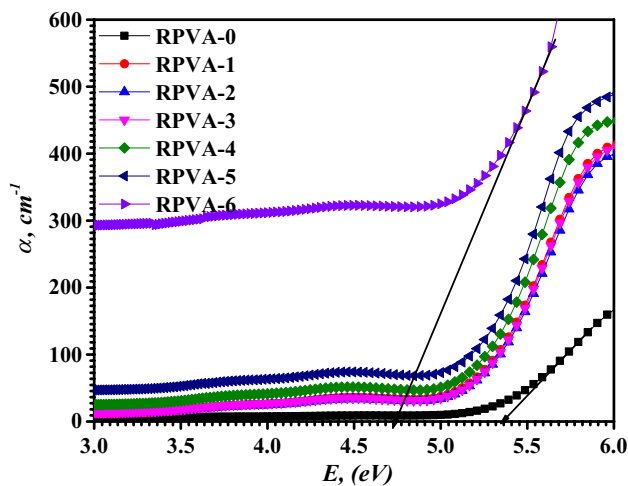

Fig. 7 The Variation of optical absorption coefficient (α) with the photon energy ($E = h\nu$) of pristine and Ru doped PVAL polymer films

By interpreting the observed absorption spectra into Tauc's plots, the optical energy band gap can be calculated. We use the frequency-dependent absorption coefficient $\alpha(\nu)$ given by Mott and Davis to translate the absorption spectrum into Tauc's plot [19]:

$$\alpha(\nu)E = K\left(E - E_g^{opt}\right)^x \tag{4}$$

where $E = h\nu$ is the energy of the incident photon, K is the factor that depends on the transition of the internal band, E_g^{opt} is the energy of the optical bandgap, and x is the index that describes how electronic transitions cause optical absorption. The x can take each of the values two or ½ for indirect and direct permitted optical transitions. The extrapolation of the linear portion of the curves to zero of $(\alpha E)^{1/x}$, provides the bandgap energy value for direct E_{gd}^{opt} and indirect E_{gi}^{opt} at the abscissa axis, as shown in Fig. 9a, b. The results for each polymer sample are listed in Table 2. E_{gi}^{opt} was dropped from 4.997 eV for RPVA-0 to 4.165 eV for RPVA-6, while E_{gd}^{opt} values are reduced from 5.610 eV to 5.149 eV, respectively. The effect of dopant to decrease the bandgap value of the polymer was observed in several works such as Li_2SO_4 in PVAL/PVP, La^{3+}-ions in PVAL, and blend polymer as illustrated in Table 2 [2, 46, 47]. This can be explained by the significant changes in the PVAL electronic structure via specific amounts of dopants [52]. The incorporated filler reduces the gap between the valence band and the conduction band, as it induces localized electronic states allowing electronic transitions with less energy [53, 54]. According to modifications in the structure of the doping polymer, the reduced band gaps with increased the Ru-content suggest an increase in PVAL film disorder.

Additionally, if the bandgap transition with Tauc's relationship is accurate; the polymer specimen's thickness possibly needs to be precisely measured, which is often not possible with a tiny thickness of polymer films. By preventing the measurement of the film's thickness, the optical bandgap's energy can be determined accurately from the absorbance data. This practice is recognized as the absorbance spectrum fitting (ASF). The optical energy band gap can be defined from the following relationship according to this approach [55, 56]:

$$A = D_1\lambda\left[\frac{1}{\lambda} - \frac{1}{\lambda_{opt}}\right]^{x-1} + D_2 \tag{5}$$

$$D_1 = \left[t(hc)^{x-1}/2.303\right]K \tag{6}$$

where h is Plank's constant, c is the speed of light, λ_{opt} is the wavelength related to the optical energy bandgap, and D_2 is a constant that considers the fraction of the incident light lost [57]. The magnitude of the optical energy band gap can be

Table 2 Fundamental absorption edge, Urbach energy, and optical energy band gap of pristine and Ru mixed PVAL films

Films	E_e (eV)	E_u (eV)	E_g^{opt}(eV) (Tauc's relation)		E_g^{opt}(eV) (ASF method)		References
			E_{gi}^{opt}	E_{gd}^{opt}	E_{gi}^{opt}	E_{gd}^{opt}	
RPVA-0	5.347	0.639	4.997	5.610	4.997	5.604	Present
RPVA-1	5.220	0.687	4.906	5.482	4.885	5.455	Present
RPVA-2	5.211	0.694	4.891	5.472	4.860	5.453	Present
RPVA-3	5.206	0.703	4.887	5.468	4.848	5.447	Present
RPVA-4	5.202	0.745	4.870	5.447	4.835	5.434	Present
RPVA-5	5.181	0.837	4.844	5.426	4.798	5.412	Present
RPVA-6	4.675	2.290	4.165	5.419	4.315	5.407	Present
PVAL:4-20wt% La^{3+}	5.12–4.59	–	4.74–4.55	–	–	–	[2]
PVAL/PVP/0.6–2 wt% Li$_2$SO$_4$	–	0.76–1.37	2.98–2.20	–	–	–	[46]
PVAL/PVP-xLa^{3+}	5.16–4.96	–	4.88–4.75	–	4.79–4.62	–	[47]
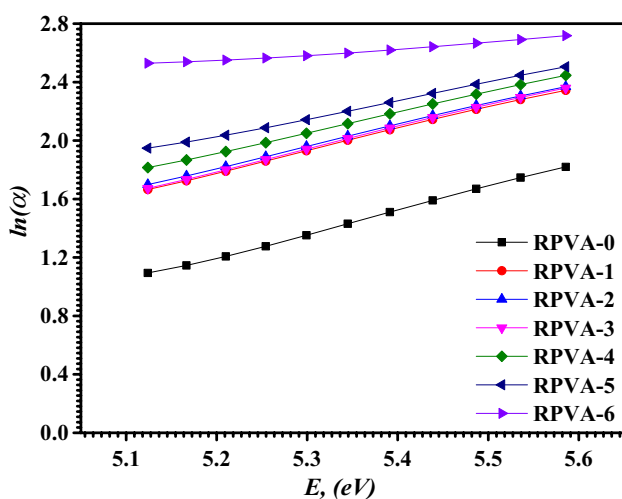
Fig. 8 The Variation of lnα with the photon energy ($E = h\nu$) of pristine and Ru doped PVAL polymer films

computed using the equation $E_g^{ASF} = hc/\lambda_{opt}$. The value of λ_{opt} can be derived from the extrapolation of the linear segment of the curve of $(A/\lambda)^{1/x}$ versus to $(1/\lambda)$, at $(A/\lambda)^{1/x} = 0$. Figure 10a, b shows the variation of $(A/\lambda)^{1/2}$, and $(A/\lambda)^2$ with λ^{-1} for indirect and direct transitions. The values of E_g^{ASF} are recorded in Table 2. Comparing Figs. 9 and 10 shows that there is a good agreement between the values of the band gaps determined from Tauc's and ASF methods. As seen in Table 2, this agreement was noticed in previously studied for La^{3+} doped PVAL/PVP-blend [47].

3.5 Limiting Optical Absorption (LOA) Performance

The film's LOA behavior was tested via both types of laser sources (green laser and He–Ne) of λ = 533 nm and 623.8 nm. Moreover, the impact of Ru-metal content was
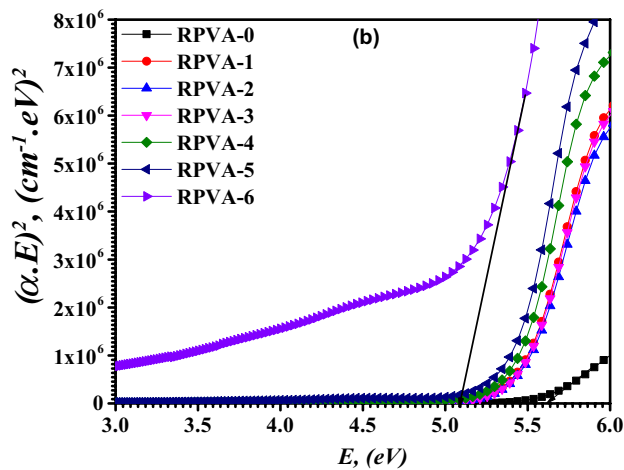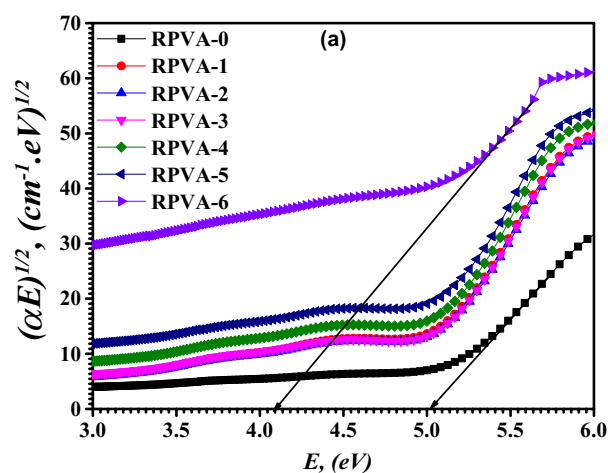
Fig. 9 **a** Indirect, and **b** direct energy band gaps of pristine and Ru doped PVAL polymer films

considered. The output power measured through a sensitive digital meter and the ratio between the outputs to input value (Normalized Power) of each source for all films are
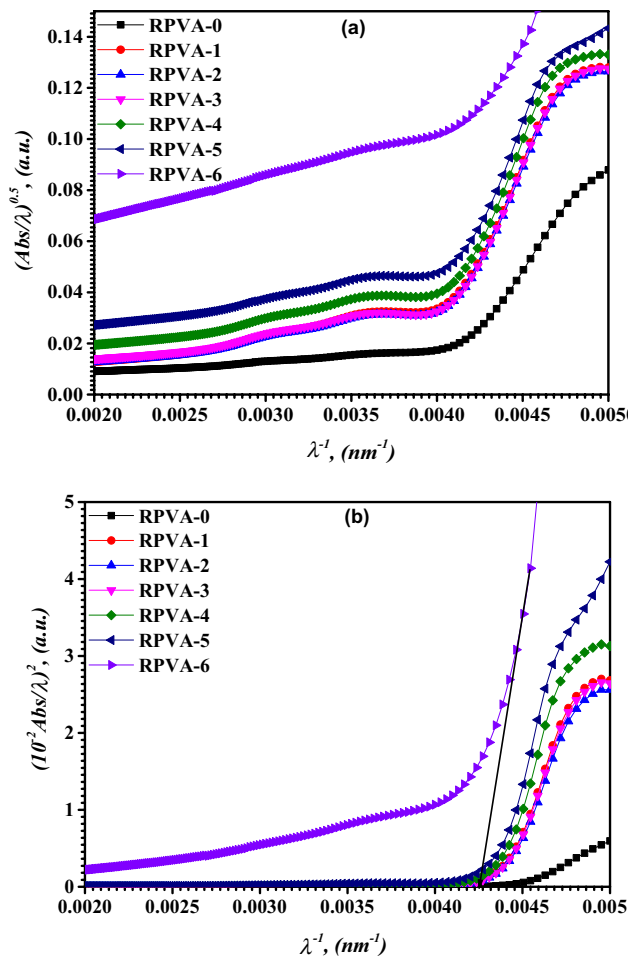
Fig. 10 Variation of **a** $(Abs.\lambda)^{1/2}$, and **b** $(Abs.\lambda)^2$ versus λ^{-1} of pristine and Ru doped PVAL films

Fig. 11 **a, b** The output (**a**) and normalized (**b**) power for pristine and Ru doped PVAL films

plotted in Fig. 11a, b. It was noticed that an insignificant diminution occurred via samples with a small content of Ru-metal. However, a substantial decrease was observed for films of higher doping. This shows the influence of Ru-metal concentration in the PVAL network on the LOA, as with the rising Ru ratio, the value of output and the normalized powers were reduced. This action is the distribution of Ru- particles over the PVAL surface, as illustrated via SEM images. Moreover, it was related to the interface interaction of the incident plane wave with Ru-metal. A similar laser behavior was earlier observed by doping PVAL with a high concentration of $CuCl_2$ salt or BiI_3 nanoparticles [17, 58]. The attenuation of laser is associated basically to the film absorption response to the incident beam wavelength. At the high Ru-metal ratio in PVAL films, the transmittance is close to approximately zero in the visible light. Thus, as a consequence of the
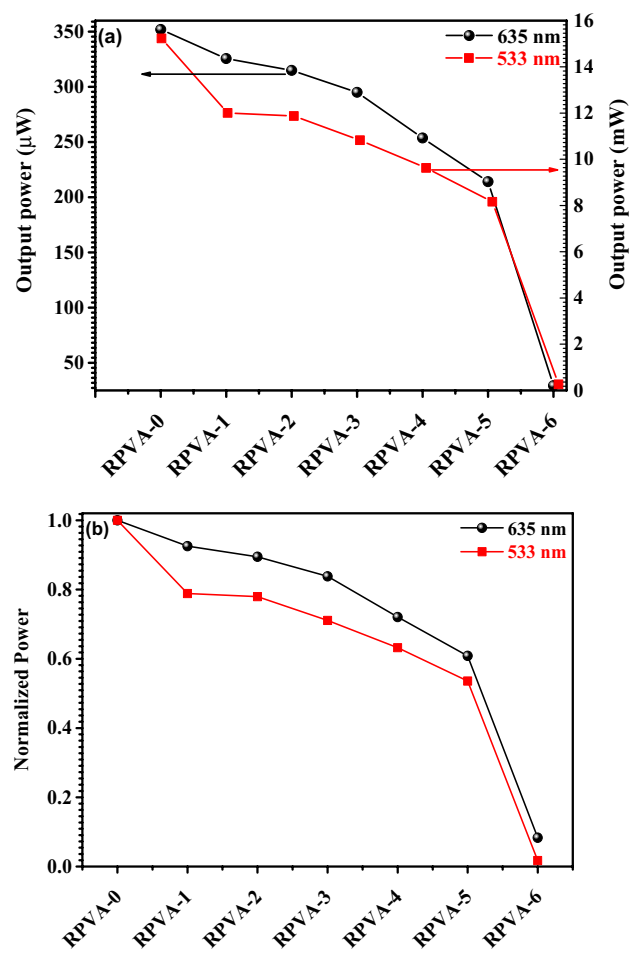
LOA, the RPVA-6 film can be applied in laser protector and photonic devices of limiting optical absorption.

3.6 Dielectric and Electrical Conductivity Study

3.6.1 Frequency Dependence of Dielectric Properties

The dielectric constant (ε') and dielectric loss (ε'') spectra for RPVA films are shown in Fig. 12a, b at room temperature, over a frequency range of 30 kHz to 10 MHz. The ε' and ε'' values reflect the electrical energy storage capacity and energy loss per cycle, respectively. The values of each of them were estimated via the expressions:

$$\varepsilon' = \frac{C(F).X(m)}{\varepsilon_o\left(F.m^{-1}\right)A\left(m^2\right)} \tag{7}$$

$$\varepsilon'' = tan\delta \times \varepsilon' \tag{8}$$
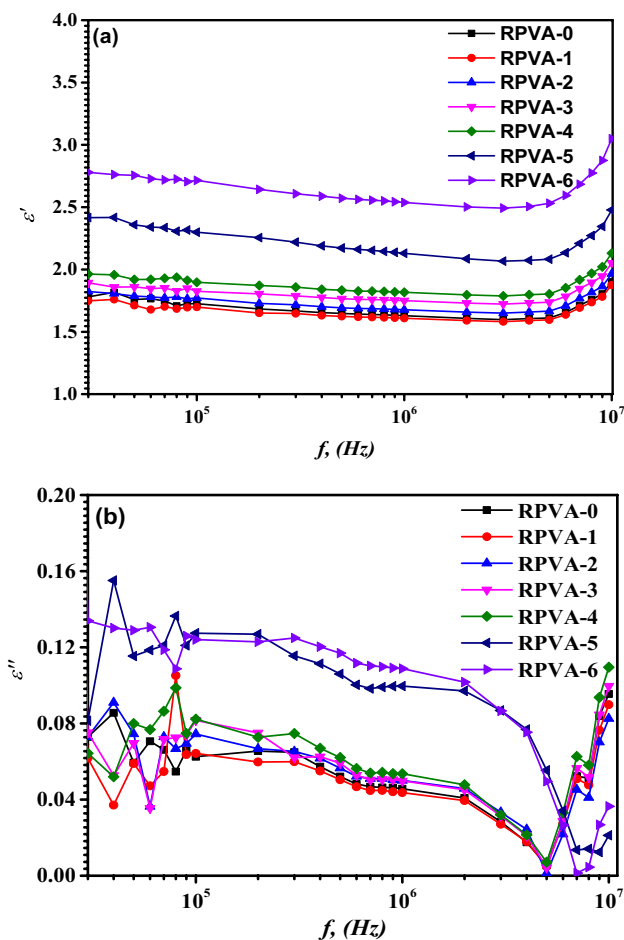
Fig. 12 Frequency dependence of **a** dielectric loss ε', and **b** dielectric loss ε''

Fig. 13 The frequency dependence of ac-conductivity of unmixed and Ru doped PVAL films

the value of the dielectric loss ε'' of as-synthesized films decreases until they reach a minimum and increases gradually at a substantially higher frequency range, as shown in Fig. 12b. The values of ε'' are small and have a similar manner of ε'. An identical manner was found by La^{3+}/PVAL and La^{3+}-doped PVDF samples [14, 64].

3.6.2 Frequency Dependence of Electrical Conductivity

Figure 13 represents the variation in the ac-conductivity (σ_{ac}), at room temperature, for RPVA films with the frequency changes from 3 kHz to 10 MHz. The conductivity increases with a frequency due to the charge carrier's mobility increased in the composite materials. Moreover, it is improved with the addition of Ru-filler. These results are related to an increase in the free conducting ions. The significant increase in conductivity for the film with higher filler content (18.5 wt% Ru) is related to the increase in the number of carriers and mobility. The frequency dependence of the ac-conductivity for unmixed and Ru doped PVAL composite films can be characterized by Jonscher's relation [65]:

$$\sigma_{DC} = \frac{d}{R \times A} \tag{9}$$

$$\sigma_{ToT.AC} = \frac{d}{Z \times A} \tag{10}$$

$$\sigma_{ToT.AC} = \sigma_{AC} + \sigma_{DC} \tag{11}$$

$$\sigma_{ac} = A\omega^x \tag{12}$$

where all symbols were defined [59]. Upon raising the frequency from 30 kHz to 3 MHz, the dielectric constant ε' values have a drastic nonlinear decrease, while ε' is substantially increased with more content of Ru-metal (Fig. 12a). Moreover, such a significant fall in the dielectric constant by growing the frequency would be related to the interfacial polarization phenomenon that exists in these composite materials at the interfaces of distinct conductivity components, as observed in several polymeric materials doped with organic and inorganic materials [60–62]. Figure 12a shows an initial decrease of the dielectric constant values of the RPVA-1 films with the introduction of Ru fillers to 0.037 wt% and then increases up to 18.5 wt%. Such dielectric measurements indicated that the addition of 0.037 wt% Ru-metal in the PVAL network significantly decreases the number of parallel dipoles in the PVAL structure. The RPVA-2 film has an ε' value of approximately 1.58 at 3 MHz, which indicates its applicability in the manufacture of electrical and microelectronic instruments at radio frequencies [63]. With an increase in the frequency from 30 kHz to 5 MHz,
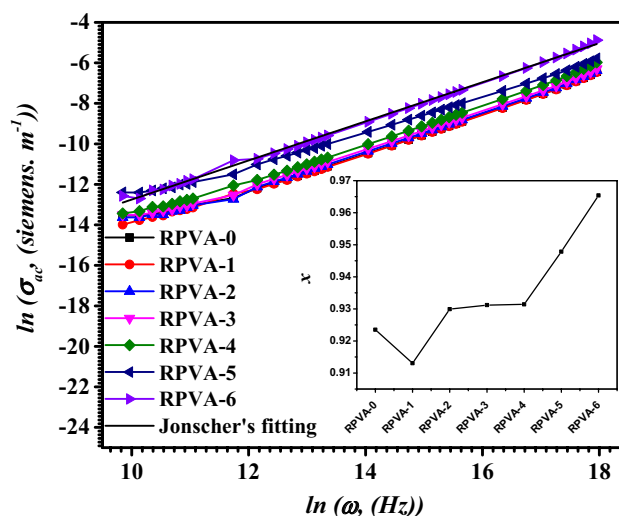
$0 \leq x \leq 1$ is a frequency exponent parameter and indicates the interactions between the charge carriers during the hopping process. Other parameters are specified elsewhere [52]. The exponent values have been determined from the slop of $ln\sigma_{ac}$ versus $ln\omega$ for all samples (see the inset of Fig. 13) which are closes proximately to 1. Factor x was increased by increasing the concentration of Ru-metal. This increase is linked to the defects motion, ions carriers, and extrinsic motions of polarization and dipoles to be the main mechanism for AC conduction [66, 67]. This result was approved via A. Bouzidi et al for CdI_2/PVAL dielectric films [65]. Therefore, the mechanism of conduction in the prepared Ru/PVAL composite films correlated to the barrier hopping model (CBH), as it can be described under the electrons hopping between localized states similar to the conduction mechanism of the di-phase TiO_2 in PVAL [66].

3.6.3 *I–V* Characteristic Curve

In electronic circuits, the varistor is a vital component used as a protective device to the circuits' other elements from excessive transient biasing. It is also known as Voltage Dependent Resistor (VDR) as it exhibits a highly nonlinear current–voltage property. The current (*I*) passing over the PVAL and its Ru-doped composites versus the applied voltage (*V*) at room temperature is shown in Fig. 14a–c. At the applied potential difference arises, the corresponding electric current increases. Moreover, by increasing the Ru-contents, the values of the current increase, as well. However, another performance has been noticed in the *I-V* characteristics for unmixed PVAL and low contents of Ru-metal films; the samples obey the Ohm's law. In high doped samples (RPVA-6), with the increment of the applied voltage (*V*), there is an increase in current (*I*), which is slowly in the beginning then increases with higher rates. The nonlinear performance of the *I–V* properties was observed and could be interpreted by two reasons. Firstly, when the applied voltage passes the nominal voltage (or breakdown voltage), the material's resistance sharply decreases, i.e., the conductance and the current increased, thereby above the 100 V which controls the barrier height and allows more charges to leap between levels than the current flow across the junction and the current values increased from nA to mA. The second reason is that the further content of the Ru-metal form physical contact networks within the polymer matrix, as these contacts could make a conduction path that may cause an increase in the current [68]. Another essential issue is that adding Ru-metal establishes localized traps in the energy band gap, causing a reduction in E_g of PVAL and increasing in the current. This behavior support consideration of the present flexible films with a high content of Ru-metal
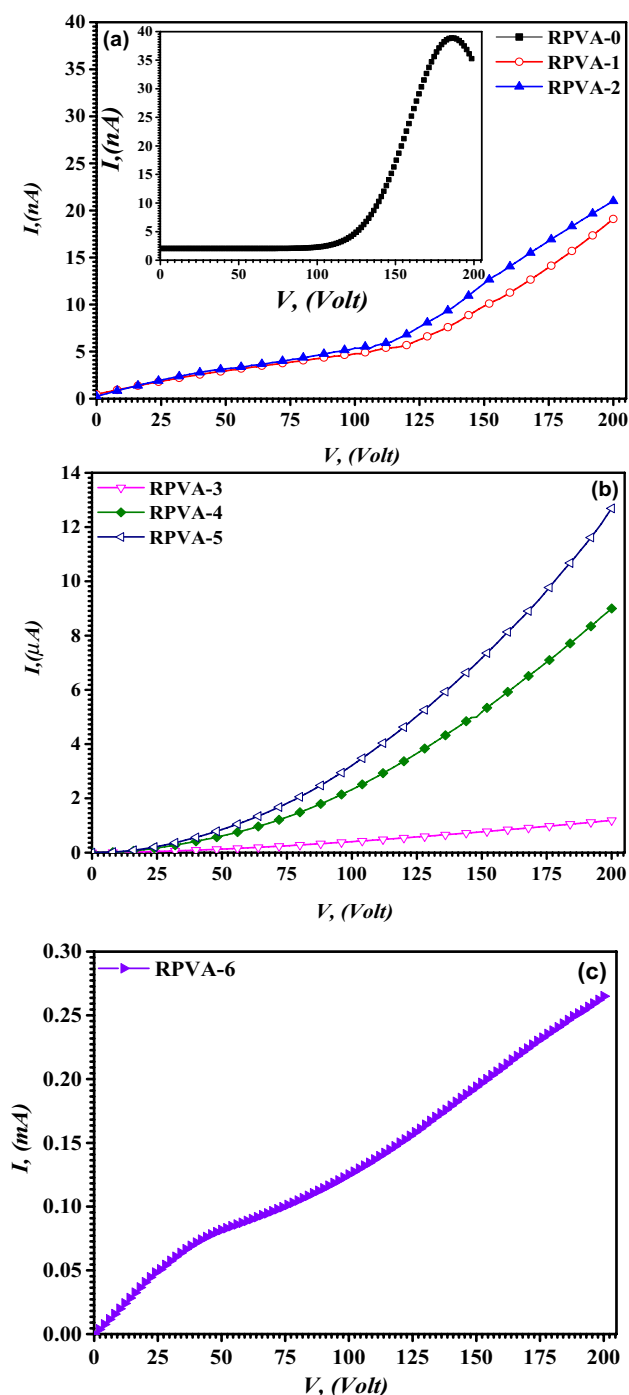

Fig. 14 a–c Variation of *I–V* plots of PVAL and Ru-mixed PVAL films

as promising composite materials in a varistor device. This behavior is in a good agreement with that reported for PVAL doped with the rare-earth ions (such as La^{3+} and Er^{3+}) at high wt% doped PVAL samples [12, 14].

4 Conclusions

Flexible polymer material with effectively incorporated Ru-metal in the PVAL matrix for optical and electrical applications was successfully prepared by casting solution techniques. The morphology and the structure parameters achieved from SEM, FTIR, and XRD measurements endorse the complexation among the PVAL chains and Ru-metal. The composites' direct and indirect optical gaps estimated using the ASF model and optical Tauc dependent absorbance relation and ASF model are slightly reduced due to Ru-metal doping and are strictly equal. The optical activation energy (E_U), calculated from the absorption coefficient, shifted from 0.63 eV to 2.29 eV. Because of Ru-metal doping, the E_U improved values were seen as raising the heterogeneity of composites. The limiting absorption (LOA) of the films measured via He–Ne and green lasers was enhanced for PVAL with high Ru-metal content. The Ru/PVAL composites have a slight increase in dielectric constant and a significant enhancement in electrical conductivity. Furthermore, the AC conductivity for mixed PVAL follows the fitting of Jonscher. The frequency exponent parameter values of composite indicate interactions between the charge carriers during the hopping process of the correlated barrier hopping model (CBH). The I–V nonlinear performance was observed for RPVA-6 film and the electric current increases with more addition of Ru content. Because of these attractive results, it could be recommended that the synthesized high-quality Ru-mixed PVAL flexible films can candidate as a polymeric varistor, optoelectronic, and CUT-OFF laser applications.

Compliance with Ethical Standards

Conflict of interest The authors declare that there is no conflict of interest in the current article.

References

1. O.G. Abdullah, S.B. Aziz, M.A. Rasheed, Results Phys. **6**, 1103–1108 (2016)
2. F.M. Ali, F. Maiz, Physica B **530**, 19–23 (2018)
3. G. Dong, X. Xiao, X. Liu, B. Qian, Z. Ma, S. Ye, D. Chen, J. Qiu, J. Nanoparticle Res. **12**(4), 1319–1329 (2010)
4. S.F. Bdewi, O.G. Abdullah, B.K. Aziz, A.A.R. Mutar, J. Inorg. Organomet. Polym. Mater. **26**(2), 326–334 (2016)
5. S. Agarwal, V.K. Saraswat, Opt. Mater. **42**, 335–339 (2015)
6. S. Daikh, F.Z. Zeggai, A. Bellil, A. Benyoucef, J. Phys. Chem. Solids **121**, 78–84 (2018)
7. J.H. Kim, J.Y. Kim, Y.M. Lee, K.Y. Kim, J. Appl. Polym. Sci. **45**(10), 1711–1717 (1992)
8. M.H. Makled, E. Sheha, T.S. Shanap, M.K. El-Mansy, J. Adv. Res. **4**(6), 531–538 (2013)
9. A.L. Saroj, R.K. Singh, Phase Transit. **84**(3), 231–242 (2011)
10. S.D. Praveena, V. Ravindrachary, R.F. Bhajantri, Polym. Compos. **37**(4), 987–997 (2016)
11. J. Zhu, Q. Li, Y. Che, X. Liu, C. Dong, X. Chen, C. Wang, Polymers **12**(2020), 453 (2020)
12. H.I. Elsaeedy, H. Elhosiny Ali, H. Algarni, I.S. Yahia, Appl. Phys. A **125**, 79 (2019)
13. H. Elhosiny Ali, Mater. Res. Express **6**(4), 045313 (2019)
14. H. Elhosiny Ali, Y. Khairy, H. Algarni, H.I. Elsaeedy, A.M. Alshehri, I.S. Yahia, J. Mater. Sci.: Mater. Electron. **29**, 20424–20432 (2018)
15. H. Elhosiny Ali, M.M. Abdel-Aziz, H. Algarni, I.S. Yahia, Mater. Res. Express **6**(8), 085334 (2019)
16. H. Elhosiny Ali, Y. Khairy, H. Algarni, H.I. Elsaeedy, A.M. Alshehri, H. Alkharis, I.S. Yahia, Opti. Quantum Electron. **51**(2), 47 (2019)
17. M.M. Abdel-Aziz, H. Algarni, A.M. Alshehri, I.S. Yahia, H. Elhosiny Ali, Mater. Res. Express **6**(12), 125321 (2019)
18. H. Elhosiny Ali, Y. Khairy, Physica B **572**, 256–265 (2019)
19. Z.Q. Tou, T.W. Koh, C.C. Chan, Sens. Actuators: B **202**, 185–193 (2014)
20. S.S. Nafee, T.A. Hamdalla, S.A. Shaheen, Phase Transit. **90**(5), 439–448 (2017)
21. H.-K. Yuan, J. Ren, X.-H. Ma, Z.-L. Xu, Desalination **280**(1), 252–258 (2011)
22. S. Akhter, K. Allan, D. Buchanan, J.A. Cook, A. Campion, J.M. White, Appl. Surf. Sci. **35**(2), 241–258 (1988)
23. O.N. Tretinnikov, S.A. Zagorskaya, J. Appl. Spectrosc. **79**(4), 521–526 (2012)
24. T.A. Hanafy, Curr. Appl Phys. **8**(5), 527–534 (2008)
25. S.B. Aziz, M.A. Rasheed, S.R. Saeed, O.G. Abdullah, Int. J. Electrochem. Sci **12**, 3263–3274 (2017)
26. R.F. Bhajantri, V. Ravindrachary, A. Harisha, V. Crasta, S.P. Nayak, B. Poojary, Polymer **47**(10), 3591–3598 (2006)
27. Y. Khairy, I.S. Yahia, H. ElhosinyAli, J. Mater. Sci. Mater. Electron. **31**, 8072–8085 (2020)
28. L.S.R. Kumara, O. Sakata, S. Kohara, A. Yang, C. Song, K. Kusada, H. Kobayashi, H. Kitagawa, Phys. Chem. Chem. Phys. **18**(44), 30622–30629 (2016)
29. Y. Luo, X. Jiang, W. Zhang, X. Li, Polym. Polym. Compos. **23**(8), 555–562 (2015)
30. S.N. Madhuri, K.S. Hemalatha, K. Rukmani, J. Mater. Sci.: Mater. Electron. **30**(9), 9051–9063 (2019)
31. N.B. RithinKumar, V. Crasta, R.F. Bhajantri, B.M. Praveen, J. Polym. **2014**(2014), 846140 (2014)
32. Z.A. Alrowaili, M. Ezzeldien, M.I. Mohammed, I.S. Yahia, Results Phys. **18**, 103203 (2020)
33. K.S. Hemalatha, K. Rukmani, RSC Adv. **6**(78), 74354–74366 (2016)
34. A. Badawi, Appl. Phys. A **126**(5), 335 (2020)
35. A.A. Alhazime, M.B. Mohamed, M.H. Abdel-Kader, J. Inorg. Organomet. Polym. Mater. **29**(2), 436–443 (2019)
36. A.K. Zak, M.E. Abrishami, W.H.A. Majid, R. Yousefi, S.M. Hosseini, Ceram. Int. **37**(1), 393–398 (2011)
37. M. Abdelaziz, Physica B **406**(6), 1300–1307 (2011)
38. M.B. Mohamed, M.H. Abdel-Kader, Mater. Chem. Phys. **241**, 122285 (2020)
39. R.G. Pearson, Inorg. Chem. **27**(4), 734–740 (1988)
40. E.F.M. El-Zaidia, H.A.M. Ali, T.A. Hamdalla, A.A.A. Darwish, T.A. Hanafy, Opt. Mater. **100**, 109661 (2020)
41. Y. Khairy, M.M. Abdel-Aziz, H. Algarni, A.M. Alshehri, I.S. Yahia, H.E. Ali, Mater. Res. Express **6**(11), 115346 (2019)

42. O.G. Abdullah, S.B. Aziz, K.M. Omer, Y.M. Salih, J. Mater. Sci.: Mater. Electron. **26**(7), 5303–5309 (2015)
43. A.H. Mohamad, O.G. Abdullah, S.R. Saeed, Results Phys. **16**, 102898 (2020)
44. M.B. Mohamed, Z.K. Heiba, N.G. Imam, J. Mol. Struct. **1163**, 442–448 (2018)
45. S.B. Aziz, M.A. Rasheed, A.M. Hussein, H.M. Ahmed, Mater. Sci. Semicond. Process. **71**, 197–203 (2017)
46. S.B. Aziz, O.G. Abdullah, A.M. Hussein, R.T. Abdulwahid, M.A. Rasheed, H.M. Ahmed, S.W. Abdalqadir, A.R. Mohammed, J. Mater. Sci.: Mater. Electron **28**(10), 7473–7479 (2017)
47. S. Prasher, M. Kumar, S. Singh, Int. J. Polym. Anal. Charact. **19**(3), 204–211 (2014)
48. E. Sheha, H. Khoder, T.S. Shanap, M.G. El-Shaarawy, M.K. El Mansy, Optik **123**(13), 1161–1166 (2012)
49. M. Halder, A.K. Meikap, J. Mater. Sci.: Mater. Electron. **30**(5), 4792–4806 (2019)
50. K.N. Shilpa, K.S. Nithin, S. Sachhidananda, B.S. Madhukar, Siddaramaiah, J. Alloys Compd. **694,** 884–891 (2017)
51. S.B. Aziz, R.B. Marif, M.A. Brza, A.N. Hassan, H.A. Ahmad, Y.A. Faidhalla, M.F.Z. Kadir, Results Phys. **13**, 102220 (2019)
52. H.M. Zidan, E.M. Abdelrazek, A.M. Abdelghany, A.E. Tarabiah, J. Mater. Res. Technol. **8**(1), 904–913 (2019)
53. Y.-Q. Li, S.-Y. Fu, Y. Yang, Y.-W. Mai, Chem. Mater. **20**(8), 2637–2643 (2008)
54. J. Rozra, I. Saini, A. Sharma, N. Chandak, S. Aggarwal, R. Dhiman, P.K. Sharma, Mater. Chem. Phys. **134**(2), 1121–1126 (2012)
55. F.M. Ali, R.M. Kershi, J. Mater. Sci.: Mater. Electron. **31**(3), 2557–2566 (2020)
56. K.M. Kaky, G. Lakshminarayana, S.O. Baki, Y.H. Taufiq-Yap, I.V. Kityk, M.A. Mahdi, J. Non-Cryst. Solids **456**, 55–63 (2017)
57. L. Escobar-Alarcón, A. Arrieta, E. Camps, S. Muhl, S. Rodil, E. Vigueras-Santiago, Appl. Surf. Sci. **254**(1), 412–415 (2007)
58. H. Elhosiny Ali, Y. Khairy, Vacuum **180**, 109640 (2020)
59. H. Elhosiny Ali, Y. Khairy, Optik **178**, 90–96 (2019)
60. M.T. Ramesan, P. Jayakrishnan, T. Anilkumar, G. Mathew, J. Mater. Sci.: Mater. Electron. **29**(3), 1992–2000 (2018)
61. S. Choudhary, R.J. Sengwa, Polym. Bull. **72**(10), 2591–2604 (2015)
62. S. Choudhary, J. Mater. Sci.: Mater. Electron. **29**(12), 10517–10534 (2018)
63. P.L. Reddy, K. Deshmukh, K. Chidambaram, M.M.N. Ali, K.K. Sadasivuni, Y.R. Kumar, R. Lakshmipathy, S.K.K. Pasha, J. Mater. Sci.: Mater. Electron. **30**(5), 4676–4687 (2019)
64. A. Hassen, T.A. Hanafy, S. Elsayed, A. Himanshu, J. Appl. Phys. **110**, 114119 (2011)
65. S. More, R. Dhokne, S. Moharil, Polym. Bull. **75**(3), 909–923 (2018)
66. A. Bouzidi, W. Jilani, I.S. Yahia, H.Y. Zahran, M.A. Assiri, J. Inorg. Organomet. Polym. Mater. **30**, 3940–3952 (2020)
67. I. Morad, H. E. Ali, M.H. Wasfy, A.F. Mansour, M.M. El-Desoky, Vacuum, 109735 (2020)
68. M.Q. Al-Gunaid, A.M. Saeed, N.K. Subramani, B.S. Madhukar, J. Mater. Sci.: Mater. Electron. **28**(11), 8074–8086 (2017)